ADVANCED MATERIALS

[6] M. Tahhan, V. T. Truong, G. M. Spinks, G. G. Wallace, *Smart Mater. Struct.* **2003**, *12*, 626.
[7] J. N. Barisci, G. G. Wallace, D. R. MacFarlane, R. H. Baughman, *Electrochem. Commun.* **2004**, *6*, 22.
[8] J. N. Barisci, G. M. Spinks, G. G. Wallace, J. D. Madden, R. H. Baughman, *Smart Mater. Struct.* **2003**, *12*, 549.
[9] G. M. Spinks, G. G. Wallace, R. H. Baughman, L. Dai, in *Electroactive Polymer (EAP) Actuators as Artificial Muscles: Reality, Potential and Challenges*, 2nd Ed. (Ed: Y. Bar-Cohen), SPIE, Bellingham, WA **2001**, Ch. 8.
[10] M. S. P. Shaffer, X. Fan, A. H. Windle, *Carbon* **1998**, *36*, 1603.
[11] S. Gupta, M. Hughes, A. H. Windle, J. Robertson, *J. Appl. Phys.* **2004**, *95*, 2038.
[12] C. M. Niu, E. K. Sichel, R. Hoch, D. Moy, H. Tennent, *Appl. Phys. Lett.* **1997**, *70*, 1480.
[13] J. N. Barisci, G. G. Wallace, D. Chattopadhyay, F. Papadimitrakopoulos, R. H. Baughman, *J. Electrochem. Soc.* **2003**, *150*, E409.
[14] A. Kuznetsova, I. Popova, J. T. Yates, M. J. Bronikowski, C. B. Huffman, J. Liu, R. E. Smalley, H. H. Hwu, J. G. G. Chen, *J. Am. Chem. Soc.* **2001**, *123*, 10 699.
[15] D. B. Mawhinney, V. Naumenko, A. Kuznetsova, J. T. Yates, J. Liu, R. E. Smalley, *Chem. Phys. Lett.* **2000**, *324*, 213.
[16] H. Hiura, T. W. Ebbesen, K. Tanigaki, *Adv. Mater.* **1995**, *7*, 275.

Platinum Nanoclusters Studded in the Microporous Nanowalls of Ordered Mesoporous Carbon**

By *Won Choon Choi*, *Seong Ihl Woo*,* *Min Ku Jeon*, *Jung Min Sohn*, *Myoung Rae Kim*, and *Hee Jung Jeon*

Meso- and macroporous materials synthesized via various routes[1] are important because of their potential applications as devices,[2] catalysts,[3] quantum-electronic technologies,[4] acoustic[5] and electrical insulators,[6] and optics.[7] Much attention has been focused on the synthesis of nanostructured carbons using arc-discharge,[8] chemical vapor deposition,[9] or template-synthesis techniques.[10] These materials have been studied for their applications as adsorbents,[11] catalyst supports,[12] hydrogen-storage materials,[13] and electrode materials.[14,15] Recently, interest has increased in the fuel-cell applications of nanostructured carbons. However, even though it is relatively easy to synthesize nanostructured carbons, it is not easy to impregnate precious-metal nanoparticles into them while maintaining some degree of control of particle size and shape.

Here we describe a novel procedure to synthesize a new mesoporous platinum–carbon nanocomposite. This method is based on the pyrolysis of carbon and platinum precursors in silica mesopores such as SBA-15 in order to take advantage of the excellent size- and shape-control achievable in the synthesis of nanodispersions. It has been reported previously that pyrolysis of an organometallic Pt compound at high temperature results in Pt clusters being buried in the carbon that is not exposed to the environment.[16] However, with the method reported here we have synthesized Pt nanoclusters studded in the microporous nanowalls of ordered mesoporous carbon. We found that this material is composed of regularly interconnected PtC nanocomposite arrays, as shown in Figure 1, and can be successfully used as a methanol-tolerant cathode material in direct-methanol fuel cells (DMFC).

"Methanol crossover" through an electrolyte membrane from anode to cathode is a major problem that limits the performance of a DMFC.[17] During DMFC operation, the anode performance increases with increasing methanol concentration, but the methanol crossover rate also increases, causing degradation of the cathode performance.[18] Although the development of methanol-tolerant oxygen-reduction electrocatalysts,[19] such as transition-metal sulfides and $Ru_{1.92}Mo_{0.08}$-SeO_4, is a promising approach, a platinum electrocatalyst is generally used because of its high stability under acidic and high overpotential conditions.

The small-angle X-ray diffraction (XRD) pattern of the as-synthesized PtC nanocomposite shows three well-resolved peaks (Fig. 2a) that can be indexed as (100), (110), and (200) reflections associated with hexagonal symmetry. The pore size distribution obtained from Ar-desorption experiments (Fig. 2b) exhibits a narrow peak at 3.5 nm. The scanning electron microscopy (SEM, Fig. 2a, inset) and transmission electron microscopy (TEM, Figs. 3a,b) images reveal that the PtC nanocomposite consists of well-ordered hexagonally arrayed bundles approximately 1 μm long. The composite nanorods are 7 nm in diameter (Fig. 3b); this parameter can be controlled by varying the pore diameter of the SBA-15.[20]

It is important to control the metal-nanoparticle morphology since this is expected to determine catalytic activity.[21] The TEM images (Figs. 3a,b) reveal that most of the Pt clusters are studded inside the composite nanorods and do not block the openings of the mesopores. In the 1–5 nm range, the Pt nanoparticles are not agglomerated. During the pyrolysis process at 900 °C, the particles do not sinter into larger particles. This composite has an excellent thermal stability and durability at high temperature. For comparison, self-ordered mesoporous carbon CMK-3 was synthesized by carbonizing sucrose in an SBA-15 template,[22] and then Pt/CMK-3 was prepared by a conventional impregnation method. The TEM image (Fig. 3c) of Pt/CMK-3 shows randomly dispersed irregular Pt clusters with sizes larger than 8–10 nm. Moreover, the Pt clusters of Pt/CMK-3 are supported not only on carbon rods but are also present between adjacent arrays; this behav-

[*] Prof. S. I. Woo, W. C. Choi,[+] M. K. Jeon, J. M. Sohn, M. R. Kim, H. J. Jeon
Center for Ultramicrochemical Process Systems and
Department of Chemical and Biomolecular Engineering
Korea Advanced Institute of Science and Technology
373-1, Kusong-dong, Yusong-gu, Taejon, 305-701 (Korea)
E-mail: siwoo@kaist.ac.kr
[+] Present address: Advanced Chemical Technology Division, Korea Research Institute of Chemical Technology, Yusung P.O. Box 107, Taejon 305-600, Korea.

[**] This research was supported by the Center for Ultramicrochemical Process Systems sponsored by KOSEF (2002-2003). We also thank Prof. J. Y. Lee for recording the TEM images.

  DOI: 10.1002/adma.200400978

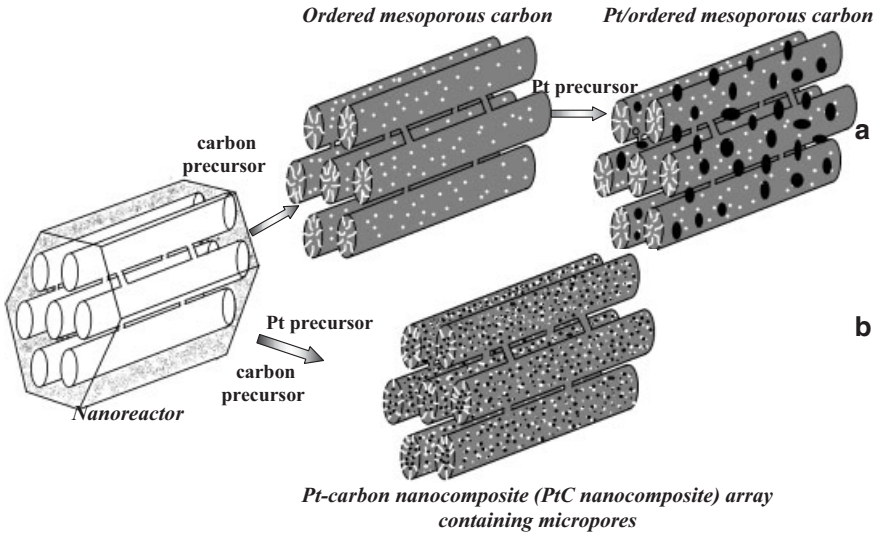

Figure 1. Schematic drawings of a) Pt/ordered mesoporous carbon prepared by a conventional impregnation method, and b) the PtC-nanocomposite array synthesized using an SBA-15 template nanoreactor.

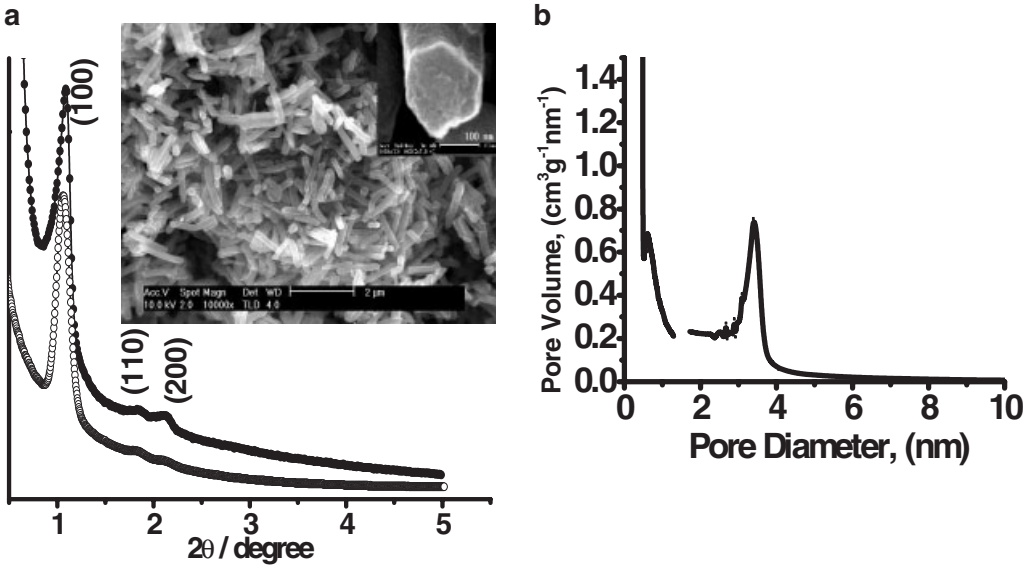

Figure 2. a) The XRD peaks of the PtC nanocomposite (24 wt.-% Pt, ○) and self-ordered mesoporous carbon (CMK-3) (●). The inset of (a) is a scanning electron microscopy image of the PtC nanocomposite. b) The pore size distribution curves of the PtC nanocomposite (12 wt.-% Pt) obtained by the Barrett–Joyner–Halenda method (>1.3 nm) and Horvath–Kawazoe analysis (0.5–1.3 nm).

ior is different from that of the PtC nanocomposite prepared by pyrolysis of carbon and platinum precursors in SBA-15 mesopores. Due to the average Pt particle size (8–10 nm) of Pt/CMK-3 and the average pore diameter (2.9 nm) of the as-synthesized CMK-3, most Pt clusters are supported on the exterior surface of CMK-3 rather than on the walls of the mesopores. The TEM image of another Pt/carbon composite (Fig. 3d), which was prepared by pyrolysis of a mixture of H_2PtCl_6 and sucrose without SBA-15 template in vacuo, shows an uncontrollable morphology of the composite containing large and irregular platinum particles.

The Brunauer–Emmett–Teller (BET) surface area of the CMK-3 measured by N_2 adsorption is 1556 $m^2 g^{-1}$, and the surface areas of the 12 % and 24 % PtC nanocomposites are 1882 $m g^{-1}$ and 1345 $m g^{-1}$ respectively, indicating that there are many micropores in the PtC nanocomposite rods into which nitrogen molecules can diffuse. Micropores 0.5–1.3 nm in diameter have also been observed by Horvath–Kawazoe analysis using Ar desorption (Fig. 2b). In order to prove that accessible Pt clusters are located inside the carbon wall, the PtC nanocomposites were treated with a bromide solution[23] to dissolve any Pt clusters located on the outer surfaces of the

ADVANCED MATERIALS

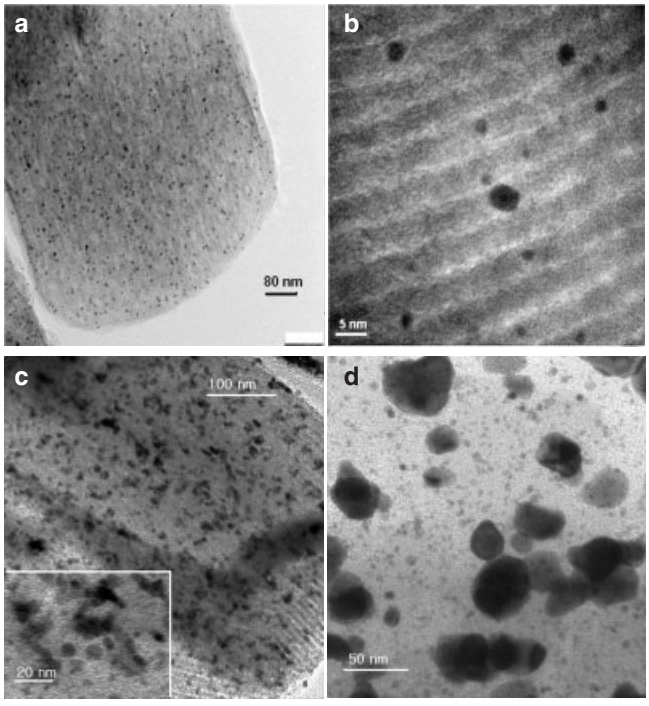

Figure 3. TEM images of the as-synthesized samples. a,b) PtC nanocomposite arrays. c) Pt/CMK-3 prepared using a conventional metal-impregnation method. d) Pt-carbon composite prepared in the same manner without SBA-15 template. The Pt contents of the samples are 24 wt.-%.

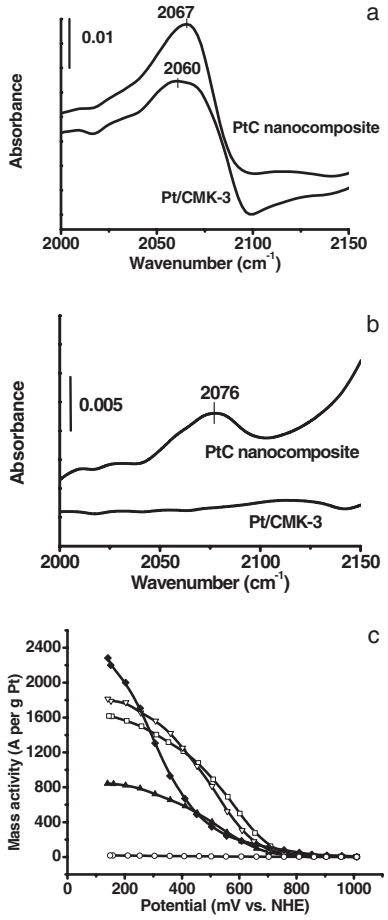

Figure 4. FTIR spectra of CO adsorbed on the PtC nanocomposite and Pt/CMK-3 a) before and b) after treatment with bromide solution. c) Electrocatalytic mass activity for oxygen reduction with 12 wt.-% Pt PtC nanocomposite (▽), 24 wt.-% Pt PtC nanocomposite (□), 24 wt.-% Pt Pt/CMK-3 (▲), and 8.5 wt.-% Pt PtC nanocomposite (◆) and Pt/CMK-3 (○) after treatment with bromide solution.

PtC nanocomposites or Pt clusters located inside micropores larger than 0.8 nm (the kinetic diameter of tetraethylammonium bromide is larger than 0.8 nm). The Pt content of the PtC nanocomposite, as measured by inductively coupled plasma–atomic emission spectroscopy (ICP–AES), was reduced from 24 wt.-% to 8.5 wt.-% after treatment with the bromide solution for 6 h. Hence, 8.5 wt.-% of the Pt is located inside the wall and is connected to micropores with diameters less than 0.8 nm. The Fourier-transform IR (FTIR) spectra (Figs. 4a,b) of CO adsorbed on the PtC nanocomposite before and after treatment with bromide solution show a band shifting from 2067 cm^{-1} to 2076 cm^{-1}, indicating that the Pt clusters studded in the microporous nanowall are not embedded and are therefore accessible to CO. In comparison, Pt/CMK-3 before treatment with bromide solution shows a band at 2060 cm^{-1}, while it does not show any CO stretching bands after the treatment. This suggests that most Pt clusters in Pt/CMK-3 exist on the exterior surface or inside mesopores. These results indicate that accessible Pt nanoclusters in micropores, which cannot be synthesized by conventional impregnation methods, are obtained by our method. The H/Pt ratio of 1.8 for the 24 wt.-% PtC nanocomposite, as obtained from H_2-chemisorption measurements, also implies that most of the Pt clusters are accessible in the meso- and micropores. The Pt nanoclusters in the micropores were also confirmed to be active in electrocatalytic oxygen reduction using a rotating disk electrode. The PtC nanocomposites before and after treatment with bromide solution and Pt/CMK-3 show the same electrocatalytic activity, whereas Pt/CMK-3 shows no activity for oxygen reduction over the whole potential window after treatment with bromide solution (Fig. 4c).

In order to confirm the methanol-tolerant characteristics of the PtC nanocomposite in a real fuel-cell system, the open-circuit voltages (OCVs) and performances of DMFC single cells with either the PtC nanocomposite or commercial Pt/C (EC-20-PTC) as cathode are shown in Figures 5a,b. A Pt reference electrode was attached to a Nafion membrane to measure the cathode performance. At various methanol concentrations and cell temperatures, the OCVs of the PtC nanocomposite are 40–60 mV higher than those of commercial Pt/C. The current density of the PtC nanocomposite is higher than that of EC-20-PTC at an activation polarization regime. With 2 M methanol at the anode, the current density of the PtC nanocomposite (112 A per gram of Pt) is 190 % that of EC-20-PTC (59 A per gram of Pt) at 810 mV (vs. reversible hydrogen electrode, RHE). For 4 M methanol at the anode, the current density of the PtC nanocomposite (89 A per gram of Pt) is 340 % that of

EC-20-PTC (26 A per gram of Pt) at 800 mV (vs. RHE). Higher OCVs and current densities indicate that the PtC nanocomposite is more methanol-tolerant than EC-20-PTC. Figures 5c,d show the oxygen-reduction activity of the PtC nanocomposite and EC-20-PTC in an O_2-saturated 1 M $HClO_4$ electrolyte with methanol. Electrooxidation of methanol by the PtC nanocomposite is almost not observed between 850 and 1000 mV (vs. normal hydrogen electrode, NHE). However, EC-20-PTC shows an electrooxidation activity of 50 A per gram of Pt in a 1 M $HClO_4$/2 M CH_3OH electrolyte at 1000 mV (vs. NHE). The ratio of the most active Pt(110) plane for methanol oxidation to the Pt(100) and Pt(111) planes decreases with a decrease in Pt particle size,[24] and the mass activity for oxygen reduction reaches a maximum when the fraction of Pt(100) and Pt(111) is also at a maximum.[25] The methanol-tolerant property of the PtC nanocomposite may be related to the characteristic orientation of the ultrafine Pt nanoclusters. It is also explained by the microporous structure of the PtC nanocomposite, which simultaneously hinders methanol diffusion while still maintaining the oxygen diffusion.

In conclusion, our basic idea was to synthesize a metal–carbon composite by pyrolysis of metal and carbon precursors in a removable silica nanoreactor. The aggregation and movement of metal precursors are hindered by polymerization or carbonization of the carbon precursors, which results in the formation of ultrafine Pt clusters even though the pyrolysis process is carried out at 900 °C. This synthetic method could be extended to the preparation of various mesoporous metal nanocomposite arrays containing micropores. In the gas-phase reaction catalyzed by various metal clusters, the diffusion of gas molecules through a regular mesopore array and through micropores at short lengths will decrease the mass-transfer limitations and tortuosity factors, resulting in an increase in the effective diffusivity of gas molecules. The higher dispersion of metal will decrease the amount of metal required to obtain the same catalytic activity per unit mass. The novel features and strategy of this study could be combined with materials processing to prepare nanostructured metal–organic/inorganic composites that will have a major impact on catalysis, optics, sensors, and electronics.[26]

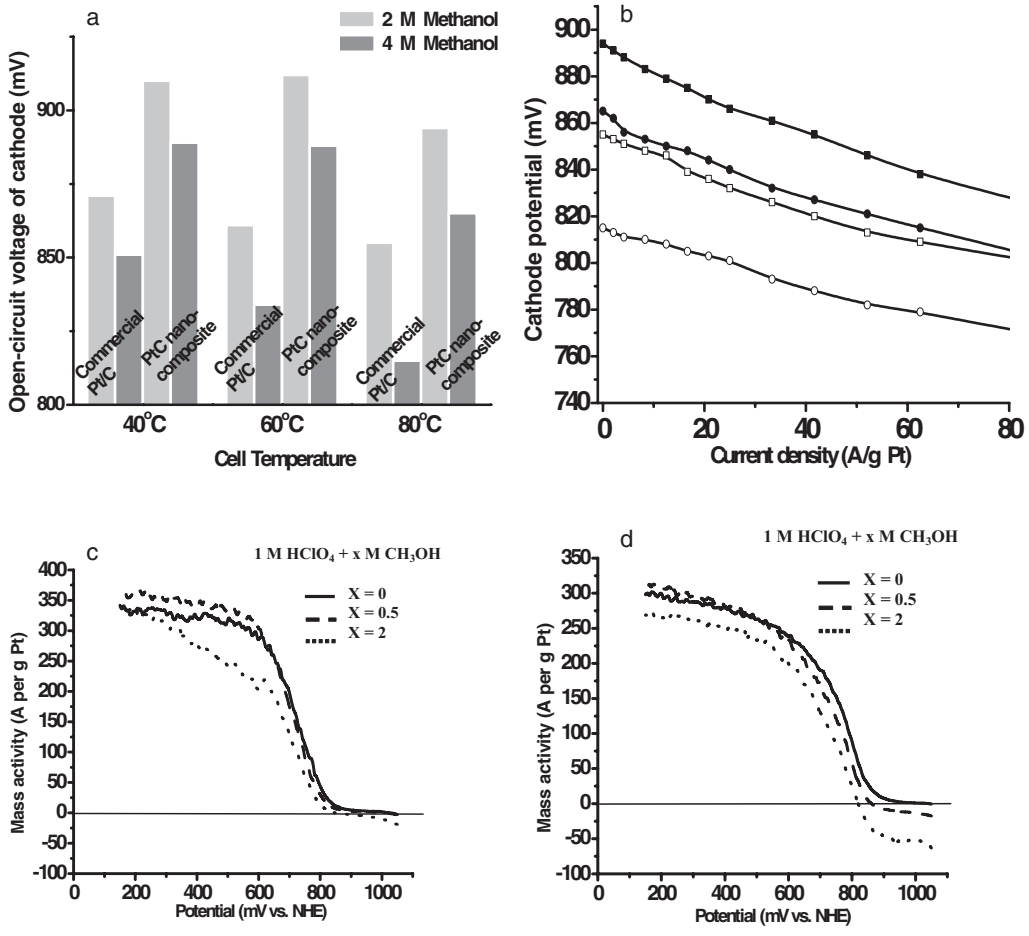

Figure 5. a) Open-circuit voltages of the cathode at various cell temperatures and methanol concentrations at the anode. b) Polarization curves of the cathode for the DMFC at 80 °C using commercial 20 wt.-% Pt/C (EC-20-PTC, open symbols) and 24 % PtC nanocomposite (filled symbols) with 2 M (squares) and 4 M (circles) methanol solutions. c) Electrocatalytic mass activity of 12 wt.-% PtC nanocomposite and d) commercial 20 wt.-% Pt/C (Electrochem Inc., EC-20-PTC) for oxygen reduction in oxygen-saturated 1 M $HClO_4$ containing x M CH_3OH (where $x = 0$, 0.5, or 2).

ADVANCED MATERIALS

Experimental

Hexagonal mesoporous SBA-15 was synthesized from Pluronic triblock copolymer (containing ethylene oxide, EO, and propylene oxide, PO, in the ratio $EO_{20}PO_{70}EO_{20}$) and tetraethyl orthosilicate ($Si(OC_2H_5)_4$) under acidic conditions [27]. Calcined SBA-15 (0.3 g) was immersed in an aqueous C_2H_5OH/H_2O (75 m; 1:1 v/v) solution containing $(NH_3)_4Pt(NO_3)_2$. After drying the slurry at 40 °C in a rotary evaporator, followed by further evacuation in vacuo at 60 °C, the resulting mixture was slurried in CH_2Cl_2 (200 mL) and dried at room temperature to introduce the Pt precursor on the outer surface of SBA-15 into the silica channels [9]. The remaining pore volume of SBA-15 was filled with sucrose and sulfuric acid. This sample was dried at 100 °C for 6 h and then at 160 °C for a further 6 h. The sample was then heated at 900 °C for 2 h under high vacuum (1×10^{-2} Pa). A 5 wt.-% hydrofluoric acid solution was used to remove the SBA-15 template.

Pt/CMK-3 was prepared by impregnating the carbon with 15.15 mM H_2PtCl_6. After drying in a rotary evaporator, the impregnated carbon support was reduced under an H_2 flow while increasing the temperature from room temperature to 310 °C (1 °C min^{-1}), and was subsequently maintained at this temperature for 2 h. The resulting Pt content in the Pt/CMK-3 was found to be 24 wt.-%.

The as-synthesized samples were treated with a mixture of Br_2 (2.5 mmol), tetraethylammonium bromide (0.5 mmol), and acetonitrile (50 g) by refluxing at 80 °C for 6 h [23]. After cooling, they were washed with acetonitrile at room temperature, and then refluxed again in acetonitrile for a further 2 h. The latter procedure was repeated three times to completely remove the dissolved Pt. Finally, they were dried at 110 °C for 12 h.

The catalyst (16 mg) and 0.16 mL of Nafion solution (5 wt.-%) were highly dispersed in 80 mL of distilled water in an ultrasonic bath. After placing 7.5 μL of this solution onto a glassy-carbon disk (3 mm in diameter), the water and alcohol were evaporated off at 90 °C. The activities were measured at 10 000 rpm and a scan rate of 50 mV s^{-1}. The electrolyte was a 1 M $HClO_4$ solution saturated with O_2. The effect of methanol addition on oxygen reduction was studied using a porous rotating disk electrode technique [17]. After dispersing 16 mg of catalyst in 16 mL of water containing 0.32 mL of Nafion solution, 15 μL of the resulting solution was transferred onto the glassy carbon disk (3 mm in diameter). The rotation speed and the scan rate were 2000 rpm and 5 mV s^{-1}, respectively. In order to compare the cathodic performance of the PtC nanocomposite with commercial Pt/Vulcan XC-72 (Electrochem Inc., EC-20-PTC), the direct-methanol fuel cell single-cell performances were studied. A catalyst slurry containing the appropriate weight of Nafion ionomer or poly(tetrafluoroethylene) was coated onto the carbon-diffusion layer of waterproofed carbon paper (Toray, TGP-H-090). PtRu black (Johnson Matthey, HiSpec 6000) was used for the anode material. The metal loadings of the anode and cathode were 5 mg cm^{-2} and 0.6 mg cm^{-2}, respectively. A membrane–electrode assembly (MEA) was fabricated by pressing a Nafion 117 membrane (DuPont) sandwiched between the as-prepared anode and cathode electrode at 120 °C for 2 min. The MEA was located between two machined graphite blocks with 4 cm^2 flow fields. The flow rate of methanol fuel and oxygen was 2 mL min^{-1} and 500 mL min^{-1}, respectively. A port for the reversible hydrogen electrode reference electrode was machined into the anode block.

Received: June 21, 2004
Final version: September 23, 2004

[1] a) B. Tian, X. Liu, B. Tu, C. Yu, J. Fan, L. Wang, S. Xie, G. D. Stucky, D. Zhao, *Nat. Mater.* **2003**, *2*, 159. b) R. A. Pai, R. Humayun, M. T. Schulberg, A. Sengupta, J.-N. Sun, J. J. Watkins, *Science* **2004**, *303*, 507. c) C. J. H. Jacobsen, C. Madsen, J. Houzvicka, I. Schmidt, A. Carlsson, *J. Am. Chem. Soc.* **2000**, *122*, 7116. d) T. Asefa, M. J. MacLachlan, N. Coombs, G. A. Ozin, *Nature* **1999**, *402*, 867. e) Y. Lu, R. Ganguli, C. A. Drewien, M. T. Anderson, C. J. Brinker, W. Gong, Y. Guo, H. Soyez, B. Dunn, M. H. Huang, J. I. Zink, *Nature* **1997**, *389*, 364. f) N. I. Kovtyukhova, T. E. Mallouk, T. S. Mayer, *Adv. Mater.* **2003**, *15*, 780. g) B. R. Martin, D. J. Dermody, B. D. Reiss, M. Fang, L. A. Lyon, M. J. Natan, T. E. Mallouk, *Adv. Mater.* **1999**, *11*, 1021.

[2] Z. Yao, H. W. C. Postma, L. Balents, C. Dekker, *Nature* **1999**, *402*, 273.

[3] a) E. S. Steigerwalt, G. A. Deluga, C. M. Lukehart, *J. Phys. Chem. B* **2002**, *106*, 760. b) J. M. Planeix, N. Coustel, B. Coq, V. Brotons, P. S. Kumbhar, R. Dutartre, P. Geneste, P. Bernier, P. M. Ajayan, *J. Am. Chem. Soc.* **1994**, *116*, 7935. c) W. C. Choi, S. I. Woo, *J. Power Sources* **2003**, *124*, 420. d) G. Che, B. B. Lakshmi, E. R. Fisher, C. R. Martin, *Nature* **1998**, *393*, 346. e) M. J. MacLachlan, N. Coombs, G. A. Ozin, *Nature* **1999**, *397*, 681. f) Y.-K. Choi, J. Zhu, J. Grunes, J. Bokor, G. A. Somorjai, *J. Phys. Chem. B* **2003**, *107*, 3340. g) Y. Ding, M. Chen, J. Erlebacher, *J. Am. Chem. Soc.* **2003**, *126*, 6876.

[4] G. L. Egan, J. Yu, C. H. Kim, S. J. Lee, R. E. Schaak, T. E. Mallouk, *Adv. Mater.* **2000**, *12*, 1040.

[5] E. Litovsky, M. Shapiro, A. Shavit, *J. Am. Ceram. Soc.* **1996**, *79*, 1366.

[6] P. Singer, *Semicond. Int.* **1996**, *19*, 88.

[7] A. Imhof, D. J. Pine, *Nature* **1997**, *389*, 948.

[8] a) T. Sugai, H. Yoshida, T. Shimada, T. Okazaki, H. Shinohara, *Nano Lett.* **2003**, *3*, 769. b) H. Li, L. Guan, Z. Shi, Z. Gu, *J. Phys. Chem. B* **2004**, *108*, 4573.

[9] Y.-L. Li, I. A. Kinloch, A. H. Windle, *Science* **2004**, *304*, 276.

[10] T. Kyotani, L.-F. Tsai, A. Tomita, *Chem. Mater.* **2000**, *7*, 1427.

[11] T. D. Power, A. I. Skoulidas, D. S. Sholl, *J. Am. Chem. Soc.* **2002**, *124*, 1858.

[12] S. H. Joo, S. J. Choi, I. Oh, J. Kwak, Z. Liu, O. Terasaki, R. Ryoo, *Nature* **2001**, *412*, 169.

[13] C. Liu, Y. Y. Fan, M. Liu, H. T. Cong, H. M. Cheng, M. S. Dresselhaus, *Science* **1999**, *286*, 1127.

[14] G. Che, B. B. Lakshmi, C. R. Martin, E. R. Fisher, *Langmuir* **1999**, *15*, 750.

[15] a) S. J. Han, Y. K. Yun, K. W. Park, Y. E. Sung, T. Hyeon, *Adv. Mater.* **2003**, *15*, 1922. b) T. Hyeon, S. Han, Y. E. Sung, K. W. Park, Y. W. Kim, *Angew. Chem. Int. Ed.* **2003**, *42*, 4352. c) W. Z. Li, C. H. Liang, W. J. Zhou, J. S. Qiu, Z. H. Zhou, G. Q. Sun, Q. Xin, *J. Phys. Chem. B* **2003**, *107*, 6292. d) J.-S. Yu, S. Kang, S. B. Yoon, G. Chai, *J. Am. Chem. Soc.* **2002**, *124*, 9382.

[16] a) N. L. Pocard, D. C. Alsmeyer, R. L. McCreery, T. X. Neenan, M. R. Callstrom, *J. Am. Chem. Soc.* **1992**, *114*, 769. b) H. D. Hutton, N. L. Pocard, D. C. Alsmeyer, O. J. A. Schueller, R. J. Spontak, M. E. Huston, W. Huang, R. L. McCreery, T. X. Neenan, M. R. Callstrom, *Chem. Mater.* **1993**, *5*, 1727.

[17] F. Maillard, M. Martin, F. Gloaguen, J.-M. Léger, *Electrochim. Acta* **2002**, *47*, 3431.

[18] a) L. Liu, C. Pu, R. Viswanathan, Q. Fan, R. Liu, E. S. Smotkin, *Electrochim. Acta* **2002**, *43*, 3657. b) B. Gurau, R. Viswanathan, R. Liu, T. Lafrenz, K. Ley, E. S. Smotkin, E. Reddington, A. Sapienza, B. C. Chan, T. E. Mallouk, S. Sarangapani, *J. Phys. Chem. B* **1998**, *102*, 9997.

[19] a) R. W. Reeve, P. A. Christensen, A. J. Dickinson, A. Hamnet, K. Scott, *Electrochim. Acta* **2000**, *45*, 4237. b) T. J. Schmidt, U. A. Paulus, H. A. Gasteiger, N. Alonso-Vante, R. J. Behm, *J. Electrochem. Soc.* **2000**, *147*, 2620. c) G. Q. Sun, J. T. Wang, R. F. Savinell, *J. Appl. Electrochem.* **1998**, *28*, 1087. d) R. W. Reeve, P. A. Christensen, A. Hamnett, S. A. Haydock, S. C. Roy, *J. Electrochem. Soc.* **1998**, *145*, 3463. e) O. Solorza-Feria, S. Citalan-Cigarroa, R. Rivera-Noriega, S. M. Fernandez-Valverde, *Electrochem. Commun.* **1999**, *1*, 585. f) N. Alanso-Vante, P. Bogdanoff, H. Tributsch, *J. Catal.* **2000**, *190*, 240. g) M. A. Priestnall, V. P. Kotzeva, D. J. Fish, E. M. Nilsson, *J. Power Sources* **2002**, *106*, 21. h) G. Q. Sun, J. T. Wang, S. Gupta, R. F. Savinell, *J. Appl. Electrochem.* **2001**, *31*, 1025. i) D. Chu, R. Jiang, *Solid State Ionics* **2002**, *148*, 591.

[20] J.-S. Lee, S. H. Joo, R. Ryoo, *J. Am. Chem. Soc.* **2002**, *124*, 1156.
[21] a) J. Zhu, Z. Kónya, V. F. Puntes, I. Kiricsi, C. X. Miao, J. W. Ager, A. P. Alivisatos, G. A. Somorjai, *Langmuir* **2003**, *19*, 4396. b) H. Wakayama, N. Setoyama, Y. Fukushima, *Adv. Mater.* **2003**, *15*, 742.
[22] S. Jun, S. H. Joo, R. Ryoo, M. Kruk, M. Jaroniec, Z. Liu, T. Ohsuna, O. Terasaki, *J. Am. Chem. Soc.* **2000**, *122*, 10712.
[23] C. Knapp, A. Obuchi, J. O. Uchisawa, S. Kushiyama, P. Avila, *Microporous Mesoporous Mater.* **1999**, *31*, 23.
[24] K. Yahikozawa, Y. Fujii, Y. Matsuda, K. Nishimura, Y. Takasu, *Electrochim. Acta* **1991**, *36*, 973.
[25] a) N. Giordano, E. Passalacqua, L. Pino, A. S. Aricò, V. Antonucci, M. Vivaldi, K. Kinoshita, *Electrochim. Acta* **1991**, *36*, 1979. b) K. Kinoshita, *J. Electrochem. Soc.* **1990**, *137*, 845.
[26] S. Komarneni, *J. Mater. Chem.* **1992**, *2*, 1219.
[27] D. Zhao, J. Feng, Q. S. Huo, N. Melosh, G. H. Fredrickson, B. F. Chmelka, G. D. Stucky, *Science* **1998**, *279*, 548.

Cap Closing of Thin Carbon Nanotubes**

By *Niels de Jonge*,* *Maya Doytcheva*, *Myriam Allioux*, *Monja Kaiser*, *Sjoerd A. M. Mentink*, *Kenneth B. K. Teo*, *Rodrigo G. Lacerda*, and *William I. Milne*

Carbon nanotubes (CNTs) are the subject of intense research due to their special properties, such as their nanometer dimensions, high aspect ratio, high Young's modulus, and high thermal and electrical conductivities.[1] One of the main hurdles for the successful application of CNTs in electronics today is the inability to precisely engineer their structure at the nanometer/atomic scale. For example, processes are under development which filter post-deposited nanotubes based on their chirality[2] in order to separate semiconducting from metallic nanotubes.[3,4] For applications such as electron emitters[5,6] and probe tips,[7,8] control is required over the structure of the nanotube tip, also referred to as its "cap". CNTs can either be open or closed directly after their growth; some processes allow the caps to be opened,[9] sharpened,[10] and even functionalized with specific chemical groups.[11] It has been proposed that open nanotubes can also be forced to close, and indications of such a process have been published.[9,12] Here, we provide experimental evidence that it is possible to close open nanotubes and we present a detailed investigation of the cap-closing mechanism of individual, thin, multiwalled CNTs (3–8 walls). The closed-cap nanotubes exhibit high current stability, which is of advantage for their use as electron sources.

A single nanotube protruding from a sharp edge was selected from an ensemble of nanotubes, prepared either by chemical vapor deposition (CVD) or arc discharge, and attached to a tungsten support tip. This nanotube was then broken by running a current through it—the break-off occurred at a weak spot along the length of the nanotube, possibly a defect in its structure (see Fig. 1). Individual, short, freestanding nanotubes on the tungsten tips were obtained using this procedure.[13] The caps of six CNTs (nos. 1–6) were imaged using transmission electron microscopy (TEM). After breaking the nanotubes, we found that four of the six displayed closed caps at their broken ends (see Fig. 2, Table 1). Note that obtaining high-resolution TEM images of freestanding individual nanotubes is very difficult, as many nanotubes are lost in the process or vibrate[8] too much to obtain atomic resolution. The nanotubes with closed caps were the ones with the smallest outer diameters and up to five walls, whilst the nanotubes with open caps had at least eight walls; dependence on the inner-wall diameter was not observed. Since all of the nanotubes

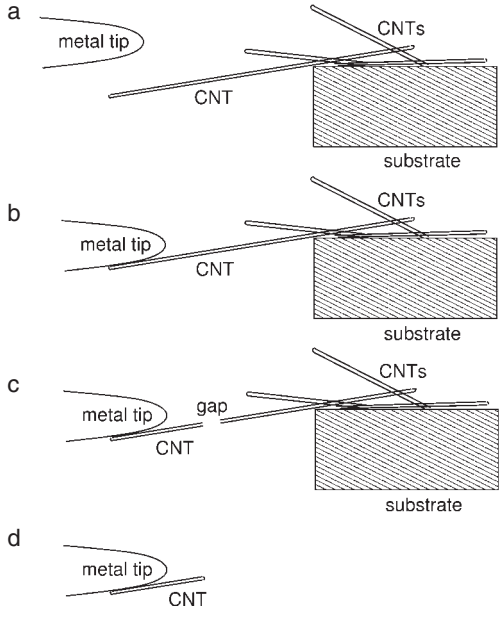

Figure 1. Mounting procedure of a CNT electron source as performed inside a scanning electron microscope. a) A CNT protruding from a thin substrate containing many nanotubes is selected and b) attached to a tungsten support tip. c) The CNT is broken by Joule heating. d) The open tube end is finally closed.

[*] Dr. N. de Jonge, Dr. M. Doytcheva, M. Allioux,[+] M. Kaiser, Dr. S. A. M. Mentink
Philips Research Laboratories
Prof. Holstlaan 4, NL-5656 AA Eindhoven (The Netherlands)
E-mail: niels.de.jonge@philips.com
Dr. K. B. K. Teo, Prof. R. G. Lacerda,[++] Prof. W. I. Milne
Department of Engineering
University of Cambridge
Trumpington Street, Cambridge CB2 1PZ (United Kingdom)
[+] Present address: Ecole Supérieure de Physique et de Chimie, Industrielles de la ville de Paris, 10 Rue Vauquelin, F-75005 Paris, France.
[++] Present address: Campus da Pampulha, Av. Antonio Carlos, 6627, CP 702, 30123-970, Belo Horizonte, MG, Brazil.

[**] We thank T. H. Oosterkamp, D. B. Peckys, and D. Tomanek for fruitful discussions, as well as G. Amaratunga, M. Meuwese, T. van Rooij, A. Teh, M. van Wely-Dieleman, and M. Yangs for experimental help, and A. G. Rinzler for kindly providing the arc-discharge nanotube sample. This work was supported by FEI Company, the Dutch Ministry of Economic Affairs, the EPSRC, and the EC.

 DOI: 10.1002/adma.200400266